Available online at www.sciencedirect.com
ScienceDirect
Journal of Catalysis 249 (2007) 24–33
JOURNAL OF CATALYSIS
www.elsevier.com/locate/jcat

Ammonia synthesis over barium-promoted cobalt catalysts supported on graphitised carbon

Wioletta Raróg-Pilecka [a], Elżbieta Miśkiewicz [a], Leszek Kępiński [b], Zbigniew Kaszkur [c], Katarzyna Kielar [a], Zbigniew Kowalczyk [a,*]

[a] *Warsaw University of Technology, Faculty of Chemistry, Noakowskiego 3, 00-664 Warsaw, Poland*
[b] *Institute of Low Temperature and Structure Research of the Polish Academy of Sciences, Okólna 2, 50-950 Wrocław, Poland*
[c] *Institute of Physical Chemistry of the Polish Academy of Sciences, Kasprzaka 44/52, 01-224 Warsaw, Poland*

Received 24 January 2007; revised 23 March 2007; accepted 24 March 2007

Available online 16 May 2007

Abstract

A group of the cobalt catalysts supported on carbon and doped with barium was prepared, characterised (by TEM, XRD, and H_2 chemisorption), and tested in ammonia synthesis under industrially relevant conditions (9.0 MPa, 400–470 °C, H_2:N_2 = 3:1). Three partly graphitised carbons (A, B, and C), with different BET surface areas ($S_A = 122$ m^2/g, $S_B = 840$ m^2/g, and $S_C = 1280$ m^2/g) were used as supports. Cobalt nitrate (index N) or cobalt acetate (index Ac) and barium nitrate were used as precursors of the active phase and a promoter precursor, respectively. TEM studies of the unpromoted Co/carbon materials treated differently (calcined in air, also reduced in hydrogen or reduced in H_2 and recalcined in air), as well as studies of the post-NH_3 synthesis catalysts promoted with barium, have shown that the specimens are heterogeneous. Hydrogen chemisorption studies of the promoted catalysts revealed that the Co dispersion in an operating system depends on the carbon texture (i.e., the higher the carbon surface area, the lower the average Co crystallite size), metal loading (i.e., a higher Co content results in a lower dispersion), and preparation procedure (i.e., reduction of the calcined Co/carbon precursor in H_2 before impregnation with barium nitrate is disadvantageous for the dispersion of the resultant catalyst, especially when highly loaded materials are prepared). Cobalt salt (nitrate vs acetate) does not influence the size of Co particles in Ba–Co/carbon. Kinetic studies of ammonia synthesis demonstrated that the surface-based reaction rates (TOF) over the Ba-promoted catalysts prepared from reduced Co/carbon precursors are lower than the rates corresponding to the catalysts derived from calcined/re-calcined precursors. The TOF values for the systems based on calcined materials (N series) proved to be independent of the average Co particle size (over the range of 5–20 nm). The apparent energy of activation for Ba–Co/carbon (92 kJ/mol) is significantly higher than that for fused iron (57 kJ/mol for KM I), but lower than that for promoted ruthenium on carbon (112 kJ/mol). Measurements of the reaction rate versus NH_3 content in the gas mixture showed in turn that cobalt is kinetically more "sensitive" to ammonia than ruthenium but is considerably less sensitive than iron. At high conversion, corresponding to 11% NH_3, the weight-based reaction rate over the most active Ba–Co/carbon catalyst (27% Co) is 7 times higher than that for iron (KM I).

Keywords: Ammonia synthesis; Cobalt catalysts; Barium promoter; Graphitic carbon support

1. Introduction

Activated carbons are commonly used as sorbents. Small amounts of the carbon materials also have applications in catalysis, mainly as supports for precious metals. The Pd, Pt, Ru, or Rh catalysts deposited on carbon are frequently used in the fine chemicals industry, preferably for hydrogenation reactions, for example, the synthesis of amines from nitro compounds or the saturation of carbon–carbon and carbon–heteroatom multiple bonds [1]. Specific examples of such reactions can be found in the literature [1–3].

The advantage of carbon is that the noble metals can be easily recovered. The spent Me/C materials can be burnt off, resulting in a concentrated ash formation [1]. Consequently, the metal recycling is simple and more economical than for sys-

* Corresponding author.
E-mail address: zbyko@ch.pw.edu.pl (Z. Kowalczyk).

0021-9517/$ – see front matter
doi:10.1016/j.jcat.2007.03.023

tems based on a conventional oxide support, such as alumina, silica, or magnesia [4].

Partly graphitised carbons obtained via high-temperature treatment (1800–2500 °C) of commercial activated carbons represent a class of materials that seems particularly promising for catalytic applications. As a result of high-temperature annealing under an inert gas atmosphere or vacuum, the oxygen complexes are almost totally removed from the carbon surface and the concentration of mineral impurities is significantly reduced. Thermally modified carbons have been shown to be excellent supports of the Pd–Au catalysts for hydrodechlorination of CCl_2F_2 [5] or Ru–Fe_3O_4 systems for the water–gas shift reaction [6,7]. Before that, however, graphitised carbons were shown to be perfect supports of ruthenium catalysts designated for ammonia synthesis [8–27]. In the last decade, the Ru/C system doped with barium and caesium was commercialised by Kellog Brown & Root [28,29]. The modern large-scale NH_3 plants operating under the KBR license are equipped with a fused iron catalyst as the first bed in a radial-flow reactor and Ru/C catalyst in three subsequent beds [28]. The combination of the catalytic materials (fused iron, ruthenium on carbon) in the KBR process proved very effective; the pressure was reduced down to 90 bar [28,29], leading to energy savings.

Numerous studies [30], including ones by us [15,31–34], have demonstrated that alkali- and/or barium-doped ruthenium catalysts supported on graphitised carbons are significantly more active in NH_3 synthesis than the traditional magnetite-based ones. Under low-pressure conditions and at high conversions, the difference between Ru/C and Fe may even exceed a factor of 300 (when the reaction rates are referred to the metal mass and a factor of 10) when they are related to the catalytic bed volume [28,33,35]. Although the Ru catalysts supported on magnesia [36–48], magnesium–aluminium spinel [49–51], MgO–CeO_2 [52], zeolites [53,54] or boron nitride [55,56] were reported to be very active as well, there is still general doubt as to whether the high cost of the noble metal is counterbalanced fully by its higher activity compared to fused iron [35]. Consequently, attempts have been made to devise a new catalytic material that is highly active and less inhibited by the ammonia product than conventional iron and also considerably cheaper than ruthenium [57–59].

Recent studies by Hagen et al. [35,60] have shown that cobalt deposited on carbon and promoted with barium is a promising catalyst for ammonia synthesis. At low pressures (10 bar), the optimised Ba–Co/C material based on commercial activated carbon also cleaned by heating at 1100 °C in a hydrogen:nitrogen = 1:9 mixture proved to be even more active than multipromoted iron (KMI, H. Topsoe) [35,60]. Our preliminary experiments [61] performed with Ba-promoted Co catalysts supported on graphitised carbon have demonstrated in turn that the properties of the system (i.e., the Co dispersion and surface-based reaction rate) may depend strongly on the unpromoted precursor pretreatment (reduction in H_2, subsequent calcinations in air). The main purpose of the present work was to explore the application potential of the Ba–Co/carbon catalysts using various graphitised carbons as supports for the metal. More specifically, the effects of cobalt loading and type of Co precursor (cobalt nitrate or acetate), as well as that of carbon texture, on ammonia synthesis rates were examined under industrially relevant conditions. In an attempt to gain insight into the properties of the cobalt catalysts, the effect of the preparation procedure reported previously [61] also was examined in detail. To investigate the morphology and structure of the materials, including the operating systems, extensive characterisation studies were performed with different samples. The specimens were characterised by chemisorption (H_2 TPD), TEM, and XRD methods. In the case of XRD, both in situ and ex situ examinations were carried out.

Table 1
Textural parameters of the carbon supports[a]

Carbon symbol	S_{BET} (m^2/g)	S_{Hg} (m^2/g)	V_{Hg} (cm^3/g)
A	122	73	0.69
B	840	179	1.08
C	1280	266	0.68

[a] S_{BET}—BET surface area; S_{Hg}, V_{Hg}—surface area and pore volume determined by mercury porosimetry.

2. Experimental

2.1. Supports and catalysts

Three carbon materials (designated A, B, and C) were used as supports for the active phase. Carbons A and B were derived from the same commercially available activated carbon (RO 08; Norit) by high-temperature treatment (1900 °C, helium, 1 h) for carbon A [62] and subsequent gasification in a CO_2 stream at 850 °C up to 23.8% mass loss for carbon B [61]. Carbon C was prepared analogously to B, through a two-step modification involving annealing at 1900 °C and gasification in CO_2 to a 27% mass loss, using the GF45 commercial product (Norit) as a starting material. The supports thus prepared were partly graphitised, as indicated by XRD, but they had different pore structures, as indicated by the low-temperature sorption of nitrogen and mercury porosimetry studies (see Table 1).

For Co/carbon, the supports were impregnated with alcoholic solutions of cobalt nitrate [$Co(NO_3)_2{\cdot}6H_2O$] or aqueous solutions of cobalt acetate [$Co(CH_3COO)_2{\cdot}4H_2O$], followed by drying in air and calcining at 220 °C for 24 h to convert the Co precursor into its oxide state (Co_3O_4). Typically, the Co loading was about 10 wt%. For higher metal content (>20%), the procedure involved impregnation and repeated calcination. In the case of catalysts deposited on carbons B and C, the calcined precursors were also reduced in flowing hydrogen at 350 °C for 24 h and, after cooling in argon to room temperature, passivated with small air pulses introduced to an argon stream. Then the passivated materials were calcined again in air (220 °C, 24 h).

To obtain the Ba-promoted systems, the preliminarily calcined samples, as well as those modified by reduction/passivation or reduction/passivation plus calcination, were impregnated with a 130 g/dm^3 aqueous solution of barium nitrate [$Ba(NO_3)_2$] at 90 °C for 16 h. Subsequently, the solid materials were separated from the hot solution, dried in air at 110 °C

Table 2
Characteristics of the Ba-promoted catalysts

Catalyst symbol	Cobalt precursor	Cobalt loading (wt%)	Modification of the unpromoted material	Barium loading ($mmol/g_{(Co+C)}$)
Ba–Co10.1$_N$/A	$Co(NO_3)_2{\cdot}6H_2O$	10.1	–	0.66
Ba–Co10.1$_N$/B	$Co(NO_3)_2{\cdot}6H_2O$	10.1	–	0.84
Ba–Co10.3$_{N(R/P)}$/B	$Co(NO_3)_2{\cdot}6H_2O$	10.3	Reduction/passivation	0.92
Ba–Co10.7$_{N(R/P+C)}$/B	$Co(NO_3)_2{\cdot}6H_2O$	10.7	Reduction/passivation + calcination	0.73
Ba–Co22.8$_N$/B	$Co(NO_3)_2{\cdot}6H_2O$	22.8	–	0.84
Ba–Co24.6$_{N(R/P)}$/B	$Co(NO_3)_2{\cdot}6H_2O$	24.6	Reduction/passivation	1.26
Ba–Co25.4$_{N(R/P+C)}$/B	$Co(NO_3)_2{\cdot}6H_2O$	25.4	Reduction/passivation + calcination	0.96
Ba–Co10.0$_{Ac}$/B	$Co(CH_3COO)_2{\cdot}4H_2O$	10.0	–	0.92
Ba–Co10.5$_{Ac(R/P)}$/B	$Co(CH_3COO)_2{\cdot}4H_2O$	10.5	Reduction/passivation	1.11
Ba–Co10.9$_{Ac(R/P+C)}$/B	$Co(CH_3COO)_2{\cdot}4H_2O$	10.9	Reduction/passivation + calcination	0.80
Ba–Co9.8$_N$/C	$Co(NO_3)_2{\cdot}6H_2O$	9.8	–	0.88
Ba–Co22.9$_N$/C	$Co(NO_3)_2{\cdot}6H_2O$	22.9	–	0.54
Ba–Co24.4$_{N(R/P)}$/C	$Co(NO_3)_2{\cdot}6H_2O$	24.4	Reduction/passivation	0.96
Ba–Co26.8$_{N(R/P+C)}$/C	$Co(NO_3)_2{\cdot}6H_2O$	26.8	Reduction/passivation + calcination	0.69

for 24 h, crushed and sieved to get a 0.2–0.63 mm fraction, and subjected to chemisorption and/or kinetic experiments.

The chemical composition of the catalysts is presented in Table 2. To readily distinguish the samples, all samples have been given uniform designations that specify in sequence the cobalt content in an unpromoted material (wt%), information on the Co precursor (N, nitrate; Ac, acetate), information on the unpromoted catalyst pretreatment (R/P, reduction plus passivation; C, additional calcination [reoxidation]) and type of carbon support (A, B, or C), for example, Co10.5$_{Ac(R/P)}$/B.

2.2. Characterisation studies

Both TEM and XRD (ex situ) were used to characterise the unpromoted cobalt oxide/carbon and Co/carbon precursors. The Ba-promoted catalysts were characterised by the H_2 chemisorption technique and XRD method and, to a lesser extent, TEM. Whereas the TEM experiments were performed with post-NH_3 synthesis Ba–Co/carbon samples, the XRD studies were performed with both postreaction specimens (ex situ examination) and specimens reduced in an XRD camera directly before the measurement (in situ XRD examinations). Furthermore, the promoted catalysts in their nonactivated state (i.e., Co/carbon samples impregnated with barium nitrate) were studied by XRD.

TEM images were recorded with a Philips CM20 Super Twin microscope, which provides 0.25-nm resolution at 200 kV. The samples for TEM studies were prepared by grinding the materials in a mortar, then dispersing them in methanol, and finally placing a droplet of the suspension on a microscope grid covered with a perforated carbon film.

X-ray powder diffraction data were collected using Bragg–Brentano geometry on the Siemens D 5000 diffractometer. Standard setting with Ni filter (1:100) and generator operating at 40 kV (40 mA) were used along with scintillation counter which measured intensity in continuous mode controlled by the DIFFRACplus software. Because of the low intensity scattered by the metal phase and peak overlap, no in depth size–strain analysis could be performed. The average size of cobalt (cobalt oxide) crystallites was determined by Scherrer's equation using the integral width of reflections fitted to the analytical Pearson VII functions. The in situ experiments were performed with a homemade environmental camera similar to that described previously [63]. The camera enabled the diffraction experiments to be performed within the same geometry as for the ex situ case. Before the XRD measurements, the sample was reduced in a flowing $H_2{:}N_2 = 3{:}1$ mixture of high purity (with nitrogen 99.999% and hydrogen 99.999%, additionally purified by being passed through an oxygen trap filled with silica-supported MnO) at 500 °C overnight, followed by cooling to room temperature.

The H_2 chemisorption measurements were carried out in a flow setup (a fully automated PEAK 4 instrument) equipped with a TCD cell and supplied with high-purity (6N) gases [64]. The details of the experimental procedure were described previously [61]. In brief, the sample (200 mg) was reduced (rereduced) in a flowing $H_2{:}Ar = 80{:}20$ mixture (40 ml/min) at 500 °C for 20 h, flushed with argon (40 ml/min) at that temperature, and cooled in argon to 150 °C. Then the Ar stream was replaced with hydrogen (40 ml/min), followed by cooling in H_2 to 0 °C. After flushing with argon (40 ml/min, 0 °C, 15 min) to remove weakly adsorbed hydrogen, the catalyst was heated in flowing Ar at a 15 °C/min temperature ramp, and the concentration of H_2 in the outlet gas was monitored (H_2 TPD). Consequently, the amount of hydrogen evolved to the gas phase could be determined by integrating the H_2 trace. The hydrogen TPD data were used for calculating the Co dispersions expressed as fraction exposed (FE)—the number of surface Co atoms related to the total number of cobalt atoms—and average sizes of metal crystallites (d_H). The $H{:}Co_s = 1{:}1$ stoichiometry [65] and formula proposed by Borodziński and Bonarowska [66] were used for determining FE and d_H, respectively.

2.3. Activity studies

Activity measurements of NH_3 synthesis were carried out in a stainless steel flow setup operating under high pressures (up to 200 bar) and supplied with an extra pure (>99.99995%) H_2:N_2 = 3:1 mixture of controlled ammonia content (0–11%). A detailed description of the apparatus and experimental procedure can be found elsewhere [64,67]. In brief, under steady-state conditions of pressure (90 bar), temperature (400–470 °C), gas flow rate (65 dm^3[STP]/h), and (x_1), the increments in NH_3 content ($x_2 - x_1$) due to the reaction over a small catalyst layer (typically 0.45 g) were measured. Based on such data, the reaction rates corresponding to the mean values of $x = (x_1 + x_2)/2$ were determined. Both the effect of temperature at constant x (8%) and that of conversion expressed by x (at constant temperature of 400 °C) on the NH_3 synthesis rate were examined. Before kinetic testing, the catalysts were reduced in a stoichiometric $H_2 + N_2$ stream at 1 bar, according to the following temperature program: 400 °C for 20 h, 470 °C for 24 h, and 520 °C for 24 h.

3. Results and discussion

3.1. Characteristics of the unpromoted systems

Three unpromoted materials—the preliminarily calcined sample derived from cobalt nitrate and carbon B (symbol $Co10.1_N$/B), the same sample additionally reduced in hydrogen and passivated (symbol $Co10.3_{N(R/P)}$/B) and that subsequently calcined (reoxidised) in air ($Co10.7_{N(R/P+C)}$/B)—were examined by TEM and XRD to determine the effects of additional operations performed with cobalt oxide on carbon. The results of TEM studies are collected in Figs. 1–3. Fig. 1 illustrates the morphology of the preliminarily calcined specimen. As seen in the low-magnification image (Fig. 1a), irregular grains of the Co-containing phase are distributed over the carbon support. The SAED pattern, shown in the inset, contains well-defined rings that can be assigned to Co_3O_4 (JCPDF Nr. 01-080-1533). The HRTEM image (Fig. 1b) shows that the grains visible in Fig. 1a are in fact clusters of 10–15 nm crystallites.

After reduction/passivation (index R/P), morphology of the material is changed, and 5–30 nm particles (mean size, 10 nm) are seen over the support (see Fig. 2a). HRTEM images (Figs. 2b and 2c) show that the particles are individual metal crystallites covered with a 2- to 3-nm layer of the oxide phase. The 0.215 nm lattice fringes visible in the core of the particle correspond to (100) lattice planes of hcp cobalt, whereas the 0.47-nm fringes in the overlayer correspond to Co_3O_4(111).

Subsequent calcination (reoxidation) of the reduced sample at 220 °C in air (index R/P + C) leads to the drastic changes in morphology (see Fig. 3a). The particles exhibit strange contrast (darker at the periphery and weaker at the centre) described as torus-like [68,69] or "hollow spheroid" [70]. Each particle is composed of small crystallites, about 4–6 nm in diameter, as

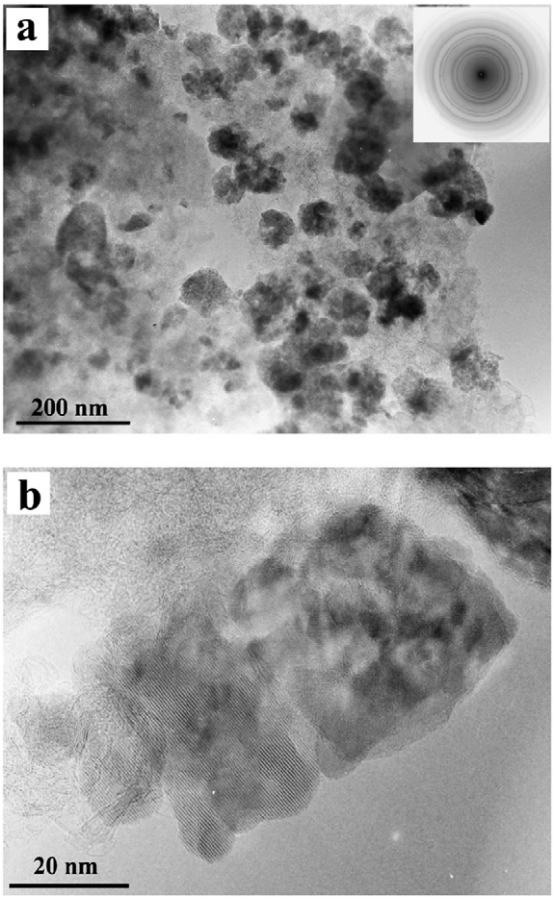

Fig. 1. Microstructure of the preliminarily calcined sample ($Co10.1_N$/B). Low magnification TEM image (a) with a SAED pattern (inset) and HRTEM image (b), showing complex, polycrystalline structure of the grains.

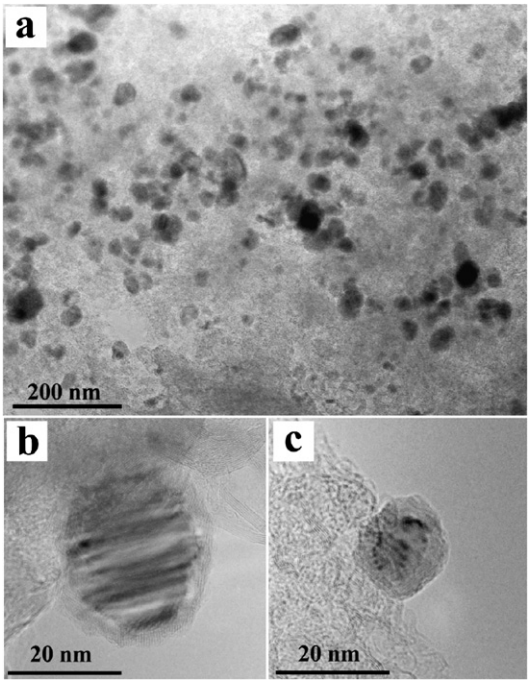

Fig. 2. Microstructure of the reduced sample ($Co10.3_{N(R/P)}$/B). Low magnification TEM image (a) and HRTEM images (b and c) showing core (metal) and shell (oxide) structure of particles.

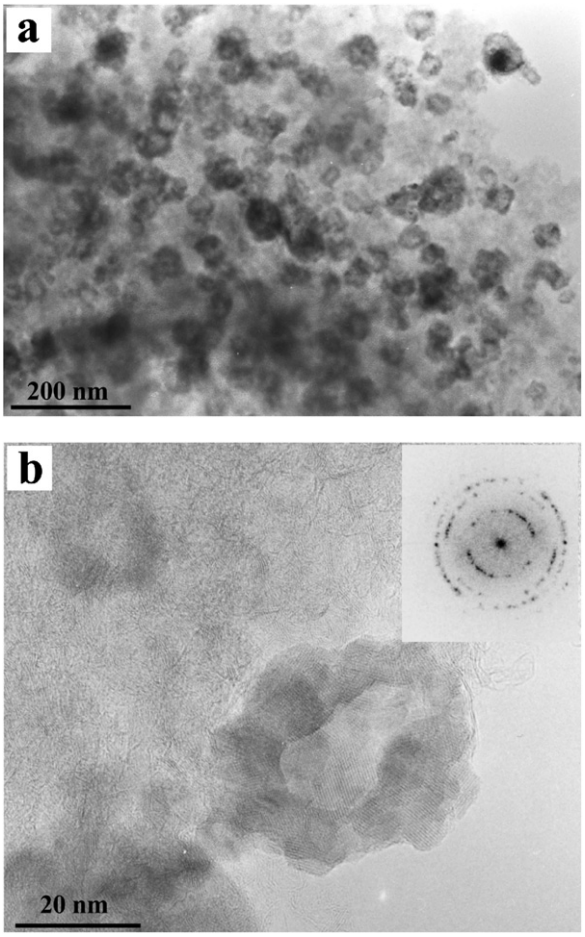

Fig. 3. Microstructure of the re-calcined sample ($Co10.7_{N(R/P+C)}$/B). Low magnification TEM image (a) and HRTEM image (b) with FFT pattern (inset) showing hollow and polycrystalline structure of cobalt oxide particles.

seen in the HRTEM image (Fig. 3b). The fast Fourier transform (FFT) pattern from the particle (shown in the inset in Fig. 3b) contains spotty rings that can be ascribed to Co_3O_4. Recent HRTEM studies of oxidation of Co [71] and Fe [72] nanocrystals provided evidence that the cause of the formation of hollow oxide particles is a large difference in the diffusion coefficients of metal and oxygen ions through the oxide layer (the outward diffusion of Co or Fe is much faster).

The results of XRD studies performed with the three unpromoted materials are shown in Fig. 4. As expected, the patterns corresponding to the calcined samples ($Co10.1_N$/B and $Co10.7_{N(R/P+C)}$/B) display a set of maxima characteristic for the Co_3O_4 phase and turbostratic carbon. The mean size of Co_3O_4 crystallites (6.5 nm) determined for the latter sample ($Co10.7_{N(R/P+C)}$/B) from line broadening is almost half that of the former sample (11 nm), in agreement with the TEM studies described above. A pattern of the reduced/passivated sample (R/P) has revealed that metallic cobalt is present in two crystallographic forms: dominating fcc (mean size, 15 nm) and hcp (about 14 nm for 100 hcp and about 4 nm for 101 hcp). Broad maxima at positions corresponding to the highest Co_3O_4 peaks suggest that some Co is already oxidised.

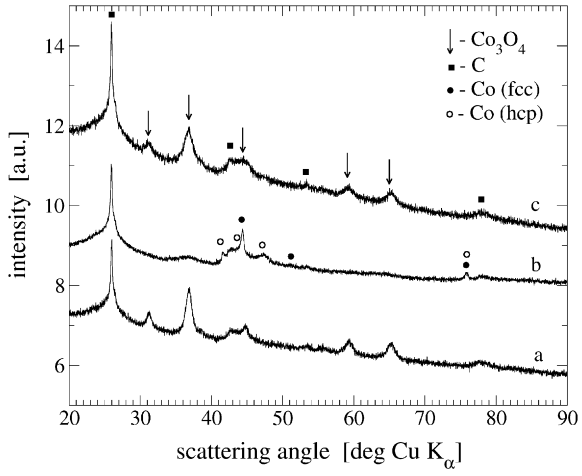

Fig. 4. XRD patterns of the unpromoted catalysts derived from cobalt nitrate and carbon B: (a) preliminarily calcined sample—$Co10.1_N$/B, (b) after reduction in H_2 and passivation—$Co10.3_{N(R/P)}$/B, and (c) after re-calcination in air–$Co10.7_{N(R/P+C)}$/B.

3.2. Characteristics of the Ba-promoted systems: Dispersion of cobalt

TEM studies of the Ba–$Co10.1_N$/B catalyst tested previously in NH_3 synthesis (Fig. 5) as well as studies of the postreaction Ba–$Co10.3_{N(R/P)}$/B specimen have shown that the promoted catalysts are heterogeneous. Large crystallites of metallic cobalt covered with amorphous oxide layer are accompanied by significantly smaller, poorly organised particles of cobalt oxide that was formed from fine Co crystals after exposing the post-NH_3 synthesis material to air. Because of the significant heterogeneity and complex nature of the particles, a detailed analysis of the particle size distributions could not be performed, and, consequently, mean sizes of the Co crystallites could not be estimated. Thus, the other Ba-containing catalysts were not examined by TEM.

The results of chemisorption experiments characterising the promoted materials in their active state are collected in Table 3; a typical H_2 TPD response is shown in Fig. 6. The reported H_2 TPD data indicate (see Table 3) that the cobalt dispersion depends on the carbon type (A, B, or C), metal loading (10% or 23–27%), and preparation procedure (reductive or reductive plus oxidative, treating the unpromoted precursors). The effect of cobalt salt (nitrate vs acetate) seems less important.

As can be seen in Table 3, a sequence of the cobalt dispersions (FE) determined for the promoted samples based on cobalt nitrate (N series, 10 wt% Co) and differing in the carbon type ($FE_{Ba–Co9.8N/C} > FE_{Ba–Co10.1N/B} > FE_{Ba–Co10.1N/A}$) remains in agreement with a sequence of the BET or mercury porosimetry surface areas of the carbon supports ($S_C > S_B > S_A$; see Table 1). This means that the texture of the support might be essential for the preparation of highly loaded and highly dispersed Ba–Co/carbon catalysts. Indeed, the FE value obtained for the (Ba–$Co22.9_N$/C) sample derived from the support of well-developed pore structure (carbon C) is more than twice higher (0.15 vs 0.065) than that determined for the catalyst based on low-surface area carbon A (Ba–$Co10.1_N$/A),

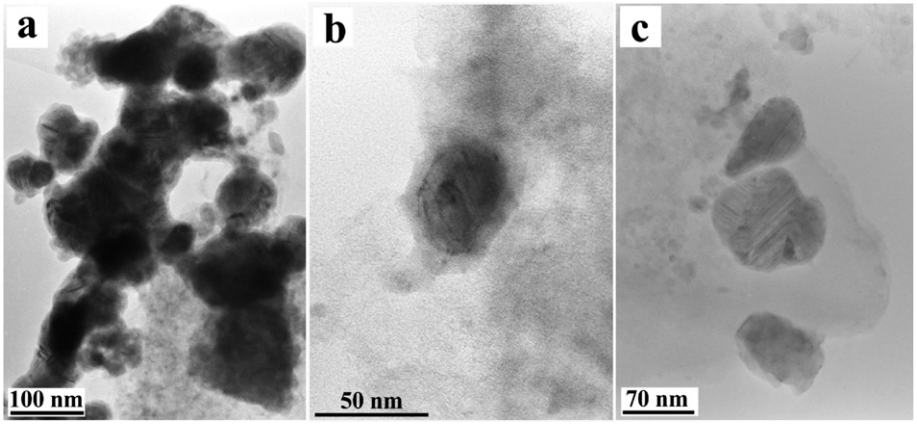

Fig. 5. TEM micrographs of the post-reaction Ba–Co10.1$_N$/B catalyst after exposure to air; (a) large aggregates of cobalt crystallites; (b) high resolution image of a single-crystal Co nanoparticle covered with an oxide layer and (c) large particles of barium carbonate that was formed from the Ba promoter.

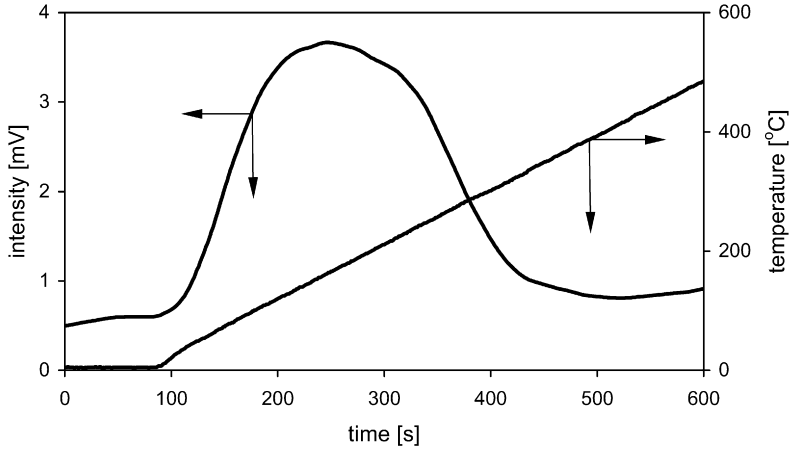

Fig. 6. Chemisorption studies. Hydrogen TPD signal for one of the promoted samples (Ba–Co26.8$_{N(R/P+C)}$/C).

Table 3
Dispersion of cobalt in the Ba–Co/C catalysts

Catalyst symbol	H_2 uptake ($\mu mol/g_{(Co+C)}$)	FE	d_H (nm)	$d_{XRD(fcc)}$[a] (nm)
Ba–Co10.1$_N$/A	56	0.065	20	13
Ba–Co10.1$_N$/B	110	0.13	9.7	14.5
Ba–Co10.3$_{N(R/P)}$/B	77	0.09	14	18.7
Ba–Co10.7$_{N(R/P+C)}$/B	135	0.15	8.4	13.
Ba–Co22.8$_N$/B	177	0.091	13.8	–
Ba–Co24.6$_{N(R/P)}$/B	78	0.037	34	–
Ba–Co25.4$_{N(R/P+C)}$/B	210	0.098	12.8	–
Ba–Co10.0$_{Ac}$/B	92	0.108	11.6	12.4
Ba–Co10.5$_{Ac(R/P)}$/B	47	0.052	24.2	18.4
Ba–Co10.9$_{Ac(R/P+C)}$/B	132	0.143	8.8	–
Ba–Co9.8$_N$/C	196	0.235	4.9	–
Ba–Co22.9$_N$/C	287	0.148	8.5	8
Ba–Co24.4$_{N(R/P)}$/C	102	0.049	25.5	12
Ba–Co26.8$_{N(R/P+C)}$/C	304	0.134	9.4	4.5

[a] d_{XRD}—determined for the post-NH_3 synthesis samples.

although the metal content in the latter system is less than half as large.

Reduction of the preliminarily calcined material before impregnation with barium nitrate always leads to a significant decrease in the number of hydrogen atoms adsorbed on the surface of the resultant catalyst, indicating decreasing Co dispersion as well (see Table 3; H_2 uptake and FE, respectively). The detrimental effect of the precursor reduction seems especially pronounced (a threefold decrease in FE) for the samples with high cobalt loading; compare the FE values determined for Ba–Co24.6$_{N(R/P)}$/B and Ba–Co22.8$_N$/B or Ba–Co24.4$_{N(R/P)}$/C and Ba–Co22.9$_N$/C. Recalcination (reoxidation) of the reduced Co/carbon specimens before barium deposition results in increased FE (see Table 3) up to the level characteristic of the systems derived from freshly calcined precursors—the barium doped-catalysts based on cobalt nitrate or, to an even greater degree, the catalyst prepared from cobalt acetate.

The above-described chemisorption studies of the Ba-promoted catalysts differing in the unpromoted precursor used (Co_3O_4 or Co on carbon) are consistent with the XRD results. Both in situ (Fig. 7) and ex situ (Fig. 8) XRD experiments performed with samples of the promoted catalysts deposited on carbon C (with highly loaded catalysts studied by XRD) demonstrate that the Co peaks corresponding to the specimen prepared from a reduced Co/C precursor (sample Ba–Co24.4$_{N(R/P)}$/C—trace b) are narrower and more distinct than those corresponding to its competitors based on the oxidised materials (Ba–Co22.9$_N$/C—trace a and Ba–

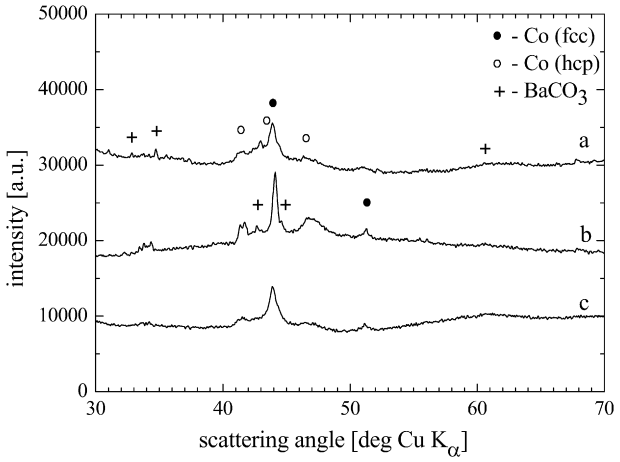

Fig. 7. XRD patterns of the promoted catalysts after their in situ reduction in a $H_2 + N_2$ mixture: (a) Ba–Co22.9$_N$/C, (b) Ba–Co24.4$_{N(R/P)}$/C, and (c) Ba–Co26.8$_{N(R/P+C)}$/C; the average cobalt crystallite sizes are 5, 8, and 6 nm for (a), (b), and (c), respectively.

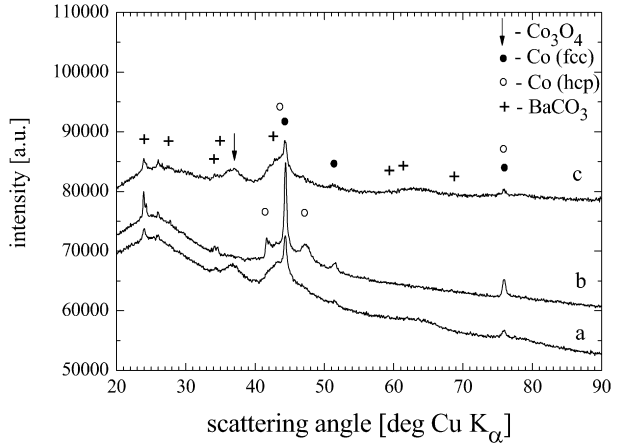

Fig. 8. XRD patterns (ex situ studies) of the promoted catalysts previously tested in NH_3 synthesis: (a) Ba–Co22.9$_N$/C, (b) Ba–Co24.4$_{N(R/P)}$/C, and (c) Ba–Co26.8$_{N(R/P+C)}$/C; the average Co crystal sizes of 8, 12, and 4.5 nm were determined from line broadening for (a), (b), and (c), respectively.

Co26.8$_{N(R/P+C)}$/C—trace c). The difference is reflected in the average crystallite sizes calculated from line broadening; the Co crystals in Ba–Co24.4$_{N(R/P)}$/C are larger than those determined for the other two materials (see Fig. 7 and the d_{XRD} data in Table 3). In addition, the ex situ examinations (Fig. 8) reveal that the patterns of the latter specimens (Ba–Co22.9$_N$/C and Ba–Co26.8$_{N(R/P+C)}$/C) expose broad maxima at positions corresponding to the highest Co_3O_4 peak (37°). This means that the samples prepared from the oxide precursors have a large fraction of very small Co crystallites that may be readily oxidised in air because of their high reactivity. In contrast, larger (and thus less reactive) Co particles in Ba–Co24.4$_{N(R/P)}$/C are probably covered with an amorphous oxide layer on exposure to air, without Co_3O_4 bulk-phase formation.

The origin of the difference in dispersions (d_H) determined for the Ba-doped catalysts based on the calcined/recalcined precursors from one side and for catalysts based on the reduced/passivated materials from the other side is unclear. The

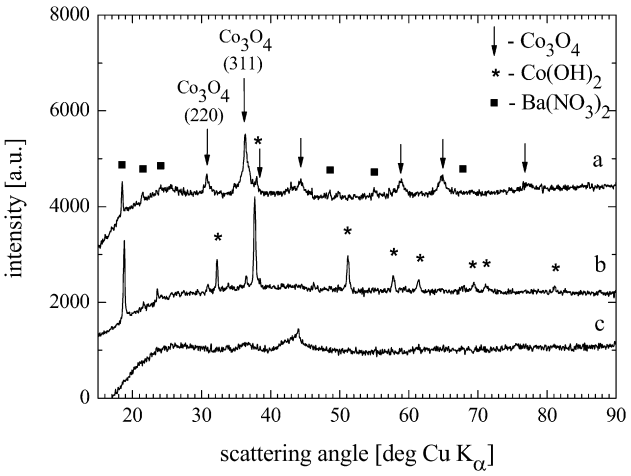

Fig. 9. XRD patterns of the Co/C systems impregnated with barium nitrate: (a) $Ba(NO_3)_2$–Co22.9$_N$/C, (b) $Ba(NO_3)_2$–Co24.4$_{N(R/P)}$/C, and (c) $Ba(NO_3)_2$–Co26.8$_{N(R/P+C)}$/C. Whereas patterns (a) and (c) show reflections of Co_3O_4, pattern (b) shows reflections of cobalt hydroxide as the only Co-containing phase.

results of additional XRD studies (Fig. 9) performed with the three highly loaded Ba–Co/C systems before their activation in an NH_3 synthesis reactor (Co/C samples impregnated with barium nitrate) provide important information. As expected, Co_3O_4 is the only cobalt-containing phase in the specimens derived from the calcined (trace a in Fig. 9) and recalcined (trace c in Fig. 9) precursors. Broad maxima (see Fig. 9) at positions corresponding to Co_3O_4 (311) or (220) indicate that the crystallites are very small; the average sizes of about 6 nm and about 3 nm result from Co_3O_4 (311) line broadening for $Ba(NO_3)_2$–Co22.9$_N$/C and $Ba(NO_3)_2$–Co26.8$_{N(R/P+C)}$/C, respectively. In contrast, the pattern of the specimen prepared from the reduced Co/C precursor [the $Ba(NO_3)_2$–Co24.4$_{N(R/P)}$/C sample—trace b in Fig. 9] does not reflect the precursor state. Instead of reflections corresponding to metallic cobalt, reflections of cobalt hydroxide are clearly seen in the pattern. The new phase [$Co(OH)_2$] had to be formed from metallic Co when impregnating the precursor with an aqueous solution of barium nitrate at elevated temperature, $Co + 2H_2O = Co(OH)_2 + H_2$. Because cobalt hydroxide in the $Ba(NO_3)_2$–Co24.4$_{N(R/P)}$/C material is well crystallised (average crystal size 40 nm), much more so than the cobalt oxide (Co_3O_4) in the other two materials (6 and 3 nm), the Co particles formed on activation of the former specimen in hydrogen are also larger ($d_H = 25.5$ nm; see Table 3) than those in the latter specimens ($d_H = 8.5$ and 9.4 nm, respectively).

3.3. Catalyst activity

The most relevant results of NH_3 synthesis studies are collected in Tables 4 and 5 and Fig. 10. Table 4 presents the reaction rates determined for all of the Ba-promoted catalysts under steady-state conditions of pressure (9.0 MPa), temperature (400 °C), and ammonia content in the gas phase (8%). The unpromoted systems proved to be completely inactive, in accordance with the literature data [11,12]. Both the weight-

Table 4
Weight-based reaction rates (r) and TOFs of NH_3 synthesis at 9.0 MPa, 400 °C and 8% NH_3 in a H_2:N_2 = 3:1 mixture

Catalyst	r ($g_{NH_3}/(g_{(C+Co)}\,h)$)	TOF (1/s)
Ba–Co10.1$_N$/A	0.26	0.038
Ba–Co10.1$_N$/B	0.48	0.036
Ba–Co10.3$_{N(R/P)}$/B	0.076	0.008
Ba–Co10.7$_{N(R/P+C)}$/B	0.63	0.038
Ba–Co22.8$_N$/B	0.86	0.040
Ba–Co24.6$_{N(R/P)}$/B	0.14	0.015
Ba–Co25.4$_{N(R/P+C)}$/B	1.05	0.040
Ba–Co10.0$_{Ac}$/B	0.19	0.017
Ba–Co10.5$_{Ac(R/P)}$/B	0.06	0.010
Ba–Co10.9$_{Ac(R/P+C)}$/B	0.40	0.025
Ba–Co9.8$_N$/C	0.90	0.038
Ba–Co22.9$_N$/C	1.39	0.039
Ba–Co24.4$_{N(R/P)}$/C	0.255	0.020
Ba–Co26.8$_{N(R/P+C)}$/C	1.52	0.041
KM I	0.33	–

Table 5
Apparent energies of activation ($E_{400-430}$) determined for some of the Ba–Co/carbon catalysts at 9.0 MPa and 8% NH_3 in the gas (H_2:N_2 = 3:1)

Catalyst	$E_{400-430}$ (kJ/mol)
Ba–Co10.1$_N$/B	92
Ba–Co22.8$_N$/B	93
Ba–Co24.6$_{N(R/P)}$/B	93
Ba–Co10.9$_{Ac(R/P+C)}$/B	92
Ba–Co24.4$_{N(R/P)}$/C	92
Ba–Co26.8$_{N(R/P+C)}$/C	91
KM I	57
Ba–Cs–Ru/carbon	112[a]

[a] Determined over the range of 370–400 °C.

based reaction rates and rates expressed in terms of TOF are reported in Table 4; the latter were obtained by combining the kinetic and hydrogen chemisorption results. The apparent energies of activation for the Ba–Co/C catalysts at 8% NH_3 are collected in Table 5. Finally, Fig. 10 illustrates, in a doubly logarithmic scale (ln–ln), the effect of ammonia partial pressure in the gas on the rate of reaction at 400 °C for the most active Ba–Co/carbon system. For comparison, the data characterising the commercial fused iron catalyst (KMI, H. Topsoe) as well as those obtained previously for the promoted ruthenium on carbon are included in Fig. 10 and Tables 4 and 5.

As can be seen in Table 4, the weight-based NH_3 synthesis rates (r) over the most active, highly loaded Ba–Co/carbon catalysts are, under the chosen experimental conditions, significantly higher than the rate determined for the commercial magnetite-based system. It is also seen that the catalytic properties of cobalt surfaces (TOF of NH_3 synthesis) in Ba–Co/carbon are affected by the kind of cobalt precursor and preparation procedure used; cobalt nitrate is a significantly more advantageous precursor of metallic Co (higher TOF) than cobalt acetate. Furthermore, the reduction of the preliminarily calcined Co/carbon materials before their impregnation with barium nitrate is disadvantageous for the resultant catalysts, i.e. it leads to lowering TOF by a factor of 2–4 (see Table 4).

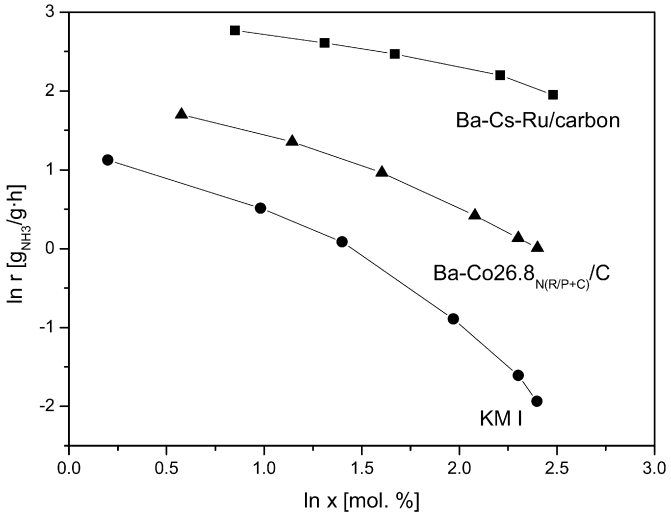

Fig. 10. Ammonia partial pressure dependencies of the reaction rates at 400 °C and 9.0 MPa for the most active cobalt catalyst Ba–Co26.8$_{N(R/P+C)}$/C, iron catalyst KM I, and ruthenium on carbon Ba–Cs-Ru9/carbon.

Two options should be considered when discussing the effect of the precursor reduction on the surface-based reaction rate (TOF) for the resultant catalysts. Either the morphology of the cobalt particles formed during the final reduction (activation) in an NH_3 synthesis reactor is controlled by the chemical form of cobalt in a post-$Ba(NO_3)_2$ impregnation material (Co_3O_4 for calcined/re-calcined precursors vs $Co(OH)_2$ for those reduced in hydrogen and passivated), or, alternatively, the Co form in $Ba(NO_3)_2$–Co/carbon controls the promotional effect of barium. According to the former concept, the promoted surfaces of cobalt crystallites formed from Co_3O_4 would be more active than surfaces of crystallites formed from $Co(OH)_2$-structure sensitivity effect. According to the latter, the Co form in the $Ba(NO_3)_2$–Co/carbon system would influence the distribution of barium between the active metal surface and surface of the carbon support in an operating catalyst. It is not possible to distinguish between the two options from the available data. However, the additional in situ XRD studies (not presented) on reduction of the unsupported Co_3O_4 and $Co(OH)_2$ materials in hydrogen demonstrate that in both cases the transformation of the cobalt precursor into its metallic state proceeds via a CoO phase as an intermediate product. Consequently, rather no difference in morphologies of the cobalt particles in the operating systems is expected, thus favouring the concept of the promoter distribution effect. In this context, a lower surface-based activity of the promoted catalysts prepared from cobalt acetate compared to those based on cobalt nitrate (see Table 4) might also be ascribed to different promotional effects of barium rather than different morphologies of cobalt crystals in the operating systems compared. Should not cobalt acetate deposited on the carbon support be fully decomposed to Co_3O_4 upon the calcination process, a barium carbonate adlayer would possibly be formed, next to Ba_xO_y, on the catalyst surface when activating the $Ba(NO_3)_2$-doped material before the NH_3 synthesis rate measurement and the overall promotional effect of barium would be weaker than that of Ba_xO_y.

In contrast to preparation procedure, the carbon type (A, B, or C) and Co dispersion do not seem to influence the properties of cobalt surfaces in NH_3 synthesis. All of the promoted catalysts derived from the calcined (recalcined) precursors based on cobalt nitrate [samples of the N and N(R/P + C) series] exhibit almost identical TOF values at 400 °C and 8% NH_3 (0.038 ± 0.002 1/s; see Table 4), although the carbon supports were different and average Co dispersions in the catalysts were different as well (see Table 3; chemisorption data). Thus, it may be concluded that ammonia synthesis on properly prepared Ba–Co/carbon catalysts is insensitive to Co particle size. Such a conclusion is undoubtedly correct for the systems of low dispersion; the average crystallite sizes in the samples varied from 5 to 20 nm (see d_H, Table 3). However, extrapolation of this conclusion down to the region of extra small (<5 nm) metal particles seems uncertain. Recent NH_3 synthesis studies of Ba- and Cs-promoted ruthenium catalysts deposited on carbon have shown [14] that the scope of extremely small crystallites (1–4 nm) is essential to the variations in a surface-based reaction rate (TOF). Further studies with the Ba–Co/carbon catalysts of high dispersion ($d_H < 5$ nm) are needed to evaluate whether the kinetic behaviour of cobalt in ammonia synthesis is similar to that of ruthenium.

The temperature dependence of the reaction rate over the cobalt catalysts, expressed via apparent energy of activation (Table 5), is independent of the type of Co precursor (nitrate or acetate) and preparation procedure. A typical value of 92 kJ/mol for cobalt at 400–430 °C and 8% NH_3 is considerably higher than that for iron (57 kJ/mol) but lower than that for ruthenium (112 kJ/mol). There are also differences among the three catalysts [i.e., Ba–Co/carbon, Ba–Ru/carbon and the magnetite-based one (iron)] in terms of the ammonia partial pressure dependencies of the reaction rate (see Fig. 10). Clearly, cobalt is kinetically more "sensitive" to ammonia than ruthenium, but is significantly less sensitive than iron. Whereas at 1% NH_3 in the gas, the weight-based reaction rate over cobalt is only slightly higher than for iron and that for ruthenium is only several times higher than for Fe (r_{Ru}:r_{Co}:r_{Fe} = 7.6:2.3:1.0), at 11% NH_3, the differences among the materials are significantly larger (r_{Ru}:r_{Co}:r_{Fe} = 51:7.0:1.0) and certainly will be even larger at higher but industrially important ammonia concentrations (15–20%), as results from the trends of the reaction rates (Fig. 10) over ruthenium, cobalt, and iron, respectively. The foregoing comparison indicates that cobalt on carbon might be a substitute for ruthenium rather than an alternative for iron. Due to the high activity, advantageous kinetic characteristics, and relatively low price of the active metal, the Ba–Co/carbon catalyst, after optimisation, might possibly replace the ruthenium-based catalyst in large-scale reactors operating with both fused iron and carbon-supported Ru [28,29]. A rather poor catalytic activity of cobalt in the reaction of carbon substrate methanation [73] seems to be an additional advantage over ruthenium.

4. Conclusion

Extensive studies (XRD, H_2 TPD, and NH_3 synthesis rate measurements) of the Ba-promoted cobalt catalysts supported on carbon have shown that both average Co particle size and catalytic properties of the Ba-doped cobalt surfaces in ammonia synthesis are dependent on the unpromoted material pretreatment. A rather low Co dispersion and low surface-based activity (TOF) for the resultant catalysts derived from the Co/carbon systems reduced in H_2 compared with those prepared from the calcined/recalcined materials should be ascribed to the changes in the former specimens forced by impregnation with an aqueous solution of barium nitrate at elevated temperature. As the impregnation step leads to conversion of metallic cobalt into well crystallised cobalt hydroxide ($Co + 2H_2O = Co(OH)_2 + H_2$), large Co particles are formed when activating the $Co(OH)_2$-containing material in an NH_3 synthesis reactor before the reaction rate measurement. Poor surface-based activity for the promoted systems based on reduced Co/carbon [or, more precisely—$Co(OH)_2$/carbon] compared with those prepared from calcined materials (Co_3O_4/carbon) seems to be a consequence of the inappropriate promoter distribution between the active phase and carbon support, rather than of the less advantageous morphology of the Co particles in the former systems during operation.

Cobalt nitrate (N) proved to be a more advantageous precursor of the active phase than cobalt acetate. Over the range of relatively large Co crystals ($d_H > 5$ nm), the catalytic properties (TOF of NH_3 synthesis) determined for the promoted catalysts derived from calcined/recalcined precursors of the N series were found to be roughly independent of dispersion. The comparison between the Ba–Co/carbon catalysts and magnetite-based commercial catalyst (KM I) indicates that the reaction rate over cobalt was more sensitive to temperature (higher activation energy for Co than for iron) and less sensitive to ammonia concentration in the gas phase. At 400 °C, 9.0 MPa and 11% NH_3, the weight-based reaction rate over the most active, highly loaded cobalt catalyst on carbon was about 7 times higher than that for KM I.

Acknowledgments

This work was carried out within the Polish Committee for Scientific Research's Research Project 3 T09 B 049 29. Z.K., W.R.-P., and E.M. thank the Foundation for Polish Science for financial support.

References

[1] E. Auer, A. Freund, J. Pietsch, T. Tacke, Appl. Catal. A 173 (1998) 259.
[2] P.N. Rylander, Hydrogenation Methods, Academic Press, New York, 1985.
[3] M. Freifelder, Practical Catalytic Hydrogenation, Wiley, New York, 1971.
[4] C. Hagelücken, Erzmetall 49 (1996) 122.
[5] M. Bonarowska, B. Burda, W. Juszczyk, J. Pielaszek, Z. Kowalczyk, Z. Karpiński, Appl. Catal. B 35 (2001) 13.
[6] A. Jedynak, Z. Kowalczyk, J. Sentek, K. Stołecki, J. Pielaszek, Przem. Chem. 80/9 (2001) 398.
[7] A. Jedynak-Koczuk, Z. Kowalczyk, Pol. J. Chem. 76 (2002) 1513.
[8] I. Rossetti, N. Pernicone, F. Ferrero, L. Forni, Ind. Eng. Chem. Res. 45 (2006) 4150.
[9] I. Rossetti, N. Pernicone, L. Forni, Catal. Today 102 (2005) 219.
[10] I. Rossetti, L. Forni, Appl. Catal. A 282 (2005) 315.

[11] I. Rossetti, N. Pernicone, L. Forni, Appl. Catal. A 208 (2001) 271.
[12] Z. Kowalczyk, J. Sentek, S. Jodzis, E. Mizera, J. Góralski, T. Paryjczak, R. Diduszko, Catal. Lett. 45 (1997) 65.
[13] S.E. Siporin, R.J. Davis, W. Raróg-Pilecka, D. Szmigiel, Z. Kowalczyk, Catal. Lett. 93 (2004) 61.
[14] W. Raróg-Pilecka, E. Miśkiewicz, D. Szmigiel, Z. Kowalczyk, J. Catal. 231 (2005) 11.
[15] W. Raróg, Z. Kowalczyk, J. Sentek, D. Składanowski, J. Zieliński, Catal. Lett. 68 (2000) 163.
[16] Ch. Liang, Z. Wei, Q. Xin, C. Li, Appl. Catal. A 208 (2001) 193.
[17] X.L. Zhenh, S.J. Zhang, J. Xu, K.M. Wei, Carbon 40 (2002) 2597.
[18] Ch. Liang, Z. Li, J. Qiu, C. Li, J. Catal. 211 (2002) 278.
[19] H.S. Zeng, K. Inazu, K. Aika, Appl. Catal. A 219 (2001) 235.
[20] Z. Zhong, K. Aika, J. Catal. 173 (1998) 535.
[21] Z. Zhong, K. Aika, Inorg. Chem. Acta 280 (1998) 183.
[22] S.M. Yunusov, E.S. Kalyuzhnaya, B.L. Moroz, S.N. Agafonova, V.A. Likholobov, V.B. Shur, J. Mol. Catal. A Chem. 165 (2001) 141.
[23] Z. Li, Ch. Liang, Z. Feng, P. Ying, D. Wang, C. Li, J. Mol. Catal. A Chem. 211 (2004) 103.
[24] S. Wu, X.F. Zheng, J.X. Chen, H.S. Zeng, N.J. Guan, Catal. Commun. 5 (2004) 639.
[25] Ch. Liang, Z. Wei, Q. Xin, C. Li, React. Kinet. Catal. Lett. 83 (2004) 39.
[26] A.S. Ivanova, E.S. Kalyuzhnaya, G.S. Litvak, E.A. Moroz, S.M. Yunusov, V.S. Lenenko, B.L. Moroz, V.B. Shur, V.A. Likholobov, Kinet. Catal. 45 (2004) 541.
[27] Y.V. Larichev, I.P. Prosvirin, D.A. Shlyapin, N.B. Shitova, P.G. Tsyrul'nikov, V.I. Bukhtiyarov, Kinet. Catal. 46 (2005) 597.
[28] R.B. Strait, Nitrogen Methanol 238 (1999) 37.
[29] R.B. Strait, S.A. Knez, in: International Conference Exhibition, Caracas, 28 February–2 March 1999.
[30] S.R. Tennison, in: J.R. Jennings (Ed.), Catalytic Ammonia Synthesis: Fundamentals and Practice, Plenum Press, New York, 1991, p. 303.
[31] Z. Kowalczyk, S. Jodzis, W. Raróg, J. Zieliński, J. Pielaszek, A. Presz, Appl. Catal. A 184 (1999) 95.
[32] Z. Kowalczyk, S. Jodzis, W. Raróg, J. Zieliński, J. Pielaszek, Appl. Catal. A 173 (1998) 153.
[33] Z. Kowalczyk, M. Krukowski, W. Raróg-Pilecka, D. Szmigiel, J. Zieliński, Appl. Catal. A 248 (2003) 67.
[34] W. Raróg, I. Lenarcik, Z. Kowalczyk, J. Sentek, M. Krukowski, J. Zieliński, Pol. J. Chem. 74 (2000) 1473.
[35] S. Hagen, R. Barfod, R. Fehrmann, C.J.H. Jacobsen, H.T. Teunissen, K. Stahl, I. Chorkendorff, J. Catal. 214 (2003) 327.
[36] F. Rosowski, O. Hinrichsen, M. Muhler, G. Ertl, Catal. Lett. 36 (1996) 229.
[37] O. Hinrichsen, F. Rosowski, A. Hornung, M. Muhler, G. Ertl, J. Catal. 165 (1997) 33.
[38] F. Rosowski, A. Hornung, O. Hinrichsen, D. Herein, M. Muhler, G. Ertl, Appl. Catal. A 151 (1997) 443.
[39] H. Bielawa, O. Hinrichsen, A. Birkner, M. Muhler, Angew. Chem. Int. Ed. 40/6 (2001) 1061.
[40] S.E. Siporin, R.J. Davis, J. Catal. 225 (2004) 359.
[41] S.E. Siporin, R.J. Davis, J. Catal. 222 (2004) 315.
[42] S.E. Siporin, B.C. McClaine, S.L. Anderson, R.J. Davis, Catal. Lett. 81 (2002) 265.
[43] K. Aika, H. Hori, A. Ozaki, J. Catal. 27 (1972) 424.
[44] K. Aika, K. Shimazaki, Y. Hattori, A. Ohya, S. Ohshima, K. Shirota, A. Ozaki, J. Catal. 92 (1985) 296.
[45] S. Murata, K. Aika, J. Catal. 136 (1992) 118.
[46] S. Murata, K. Aika, J. Catal. 136 (1992) 110.
[47] D. Szmigiel, H. Bielawa, M. Kurtz, O. Hinrichsen, M. Muhler, W. Raróg, S. Jodzis, Z. Kowalczyk, L. Znak, J. Zieliński, J. Catal. 205 (2002) 205.
[48] D. Szmigiel, W. Raróg-Pilecka, E. Miśkiewicz, M. Gliński, M. Kielak, Z. Kaszkur, Z. Kowalczyk, Appl. Catal. A 273 (2004) 105.
[49] B. Fastrup, Catal. Lett. 48 (1997) 111.
[50] T.W. Hansen, P.L. Hansen, S. Dahl, C.J.H. Jacobsen, Catal. Lett. 84 (2002) 7.
[51] C.J.H. Jacobsen, S. Dahl, P.L. Hansen, E. Tornqvist, L. Jansen, H. Topsoe, D.V. Prip, P.B. Moenshaug, I. Chorkendorff, J. Mol. Catal. A Chem. 163 (2000) 19.
[52] M. Saito, M. Itoh, J. Iwamoto, C.Y. Li, K. Machida, Catal. Lett. 106 (2006) 107.
[53] B.C. McClaine, R.J. Davis, J. Catal. 211 (2002) 379.
[54] S.E. Siporin, B.C. McClaine, S.L. Anderson, R.J. Davis, Catal. Lett. 81 (2002) 265.
[55] T.W. Hansen, J.B. Wagner, P.L. Hansen, S. Dahl, H. Topsoe, C.J.H. Jacobsen, Science 294 (2001) 1508.
[56] C.J.H. Jacobsen, J. Catal. 200 (2001) 1.
[57] R. Kojima, K. Aika, Appl. Catal. A 218 (2001) 121.
[58] R. Kojima, K. Aika, Appl. Catal. A 219 (2001) 157.
[59] C.J.H. Jacobsen, Chem. Commun. (2000) 1057.
[60] S. Hagen, R. Barfod, R. Fehrmann, C.J.H. Jacobsen, H.T. Teunissen, K. Stahl, I. Chorkendorff, Chem. Commun. (2002) 1206.
[61] W. Raróg-Pilecka, E. Miśkiewicz, M. Matyszek, Z. Kaszkur, L. Kępiński, Z. Kowalczyk, J. Catal. 237 (2006) 207.
[62] W. Raróg-Pilecka, A. Jedynak-Koczuk, J. Petryk, E. Miśkiewicz, S. Jodzis, Z. Kaszkur, Z. Kowalczyk, Appl. Catal. A 300 (2006) 181.
[63] Z. Kaszkur, J. Appl. Crystallogr. 33 (2000) 1262.
[64] W. Raróg-Pilecka, E. Miśkiewicz, S. Jodzis, J. Petryk, D. Łomot, Z. Kaszkur, Z. Karpiński, Z. Kowalczyk, J. Catal. 239 (2006) 313.
[65] R.C. Reuel, C.H. Bartholomew, J. Catal. 85 (1984) 63.
[66] A. Borodziński, M. Bonarowska, Langmuir 13 (1997) 5613.
[67] Z. Kowalczyk, Catal. Lett. 37 (1996) 173.
[68] D. Potoczna-Petru, L. Kepiński, Catal. Lett. 9 (1991) 355.
[69] D. Potoczna-Petru, J.M. Jabłoński, J. Okal, L. Krajczyk, Appl. Catal. A 175 (1998) 113.
[70] A.A. Khassin, T.M. Yurieva, G.N. Kustova, L.M. Plyasova, I.Sh. Itenberg, M.P. Demeshkina, G.K. Chermashentseva, V.F. Anufrienko, V.I. Zaikovskii, T.V. Larina, I.Yu. Molina, V.N. Parmon, J. Mol. Catal. A 168 (2001) 209.
[71] Y. Yin, R.M. Rioux, C.K. Erdonmez, S. Hughes, G.A. Somorjai, A.P. Alivisatos, Science 304 (2004) 711.
[72] C.M. Wang, D.R. Baer, L.E. Thomas, J.E. Amonette, J. Antony, Y. Qiang, G. Duscher, J. Appl. Phys. 98 (2005) 094308.
[73] A. Tomita, Y. Tamai, J. Catal. 27 (1972) 293.